Antarctic Gravity Waves: Energy and Spectral Baselines from 30-100 km using 14 years of McMurdo Lidar Observations to investigate Vertical Coupling Processes

Jackson Jandreau and Xinzhao Chu, *University of Colorado Boulder*

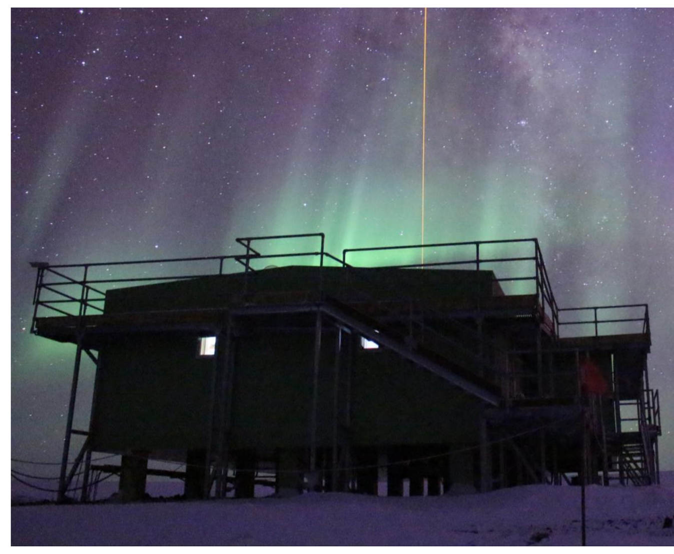

Objectives

1. Determine baseline atmospheric gravity wave lifecycle over McMurdo Station Antarctica
2. Assess the mechanisms which drive such a lifecycle as well as the variability imposed by these processes on the GW behavior
3. Use the observed GW to test theories on GW dissipation, wave generation, and various spectral development processes

Introduction

Gravity waves play a major role in transporting energy from Earth's surface to high-altitude regions, driving momentum and constituent fluxes as well as global-scale circulations. The importance and extent of these waves are still being realized and mechanisms like wave breaking and subsequent secondary-wave generation are a topic of ongoing study.

Pictured: The Arrival Heights lidar observatory at McMurdo, Antarctica with 589nm, 372nm, and 374nm channel hatches/beam-tubes shown (beams added afterwards). Since 2011, this station has monitored the atmosphere from 30-115 km, making critical discoveries about atmospheric Na/Fe metal layers.

These relatively small-scale phenomena are best studied using high-resolution instruments such as lidar, which can capture the full spectrum over a wide altitude range. The McMurdo lidar project has collected 14-years of observations, enabling the full characterization of these waves.

Methodology

Bias Elimination: The Interleaved Method of variance and spectra estimation statistically guarantees elimination of bias and noise floor

colors: (real, noise, mean-zero)

1. Retrieved parameters will have perturbations induced by noise $T = T_{bkg} + T'_{Waves} + T'_{Noise}$
$$T' = T'_{Wave} + T'_{Noise}$$
2. This noise creates a bias in variances and spectra $Var(T') = \overline{(T'_{Wave})^2} + \overline{(T'_{Noise})^2}$
$$PSD(T') \propto \langle|DFT(T'_{Wave})|^2\rangle + \langle|DFT(T'_{Noise})|^2\rangle$$
3. Separating T' into two independent datasets observing the same space, creates T' products whose T'_{Wave} correlate, and whose T'_{Noise} does not
$$T_A{}' = T'_{A,Wave} + T'_{A,Noise} \qquad T' = T'_{B,Wave} + T'_{B,Noise}$$
4. Taking the Covariance instead of Variance, and Co-Spectra instead of Spectra, create second order parameters with statistically zero bias
$$Cov(T'_A, T'_B) = \overline{T'_{A,Wave} * T'_{B,Wave}} + \overline{T'_{A,Wave}T'_{B,Noise}} + \overline{T'_{A,Wave}T'_{B,Noise}} + \overline{T'_{A,Noise} * T'_{B,Noise}}$$
$$Co\text{-}PSD(T') \propto Re\left[\overline{\begin{matrix} DFT(T'_A)DFT^*(T'_B) + DFT(T'_A)DFT^*(\Delta T_B) \\ +DFT(\Delta T_A)DFT^*(T'_B) + DFT(\Delta T_A)DFT^*(\Delta T_B)\end{matrix}}\right]$$

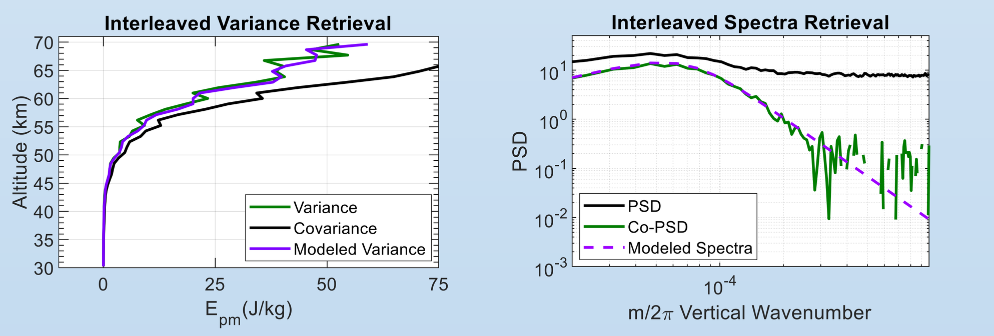

Background Removal: Careful, proper background removal is essential to wave studies, and transparency about this process is essential to readers

1. Subtract a temporal background via a 12 hr moving-mean to eliminate DC signal and non-GW wave energy, then divide perturbations by this bkg.
2. From this, estimate and subtract a 30 km moving-mean to remove remaining non-GW energy
3. Apply 6th order Butterworth filters in time and altitude with identical cutoffs to the moving-means subtractions to reinforce their effects

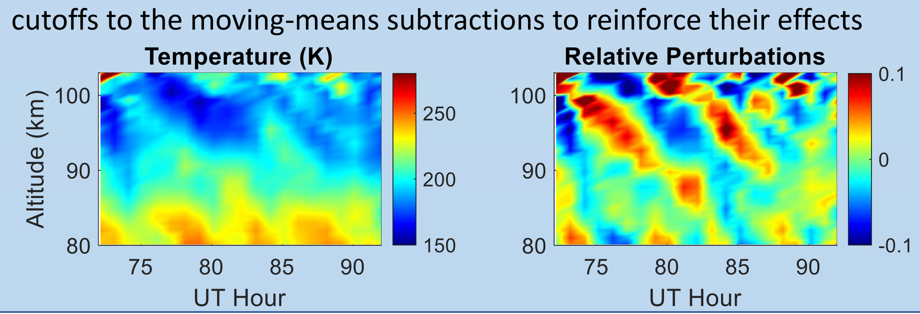

Gravity Wave Energy Baselines

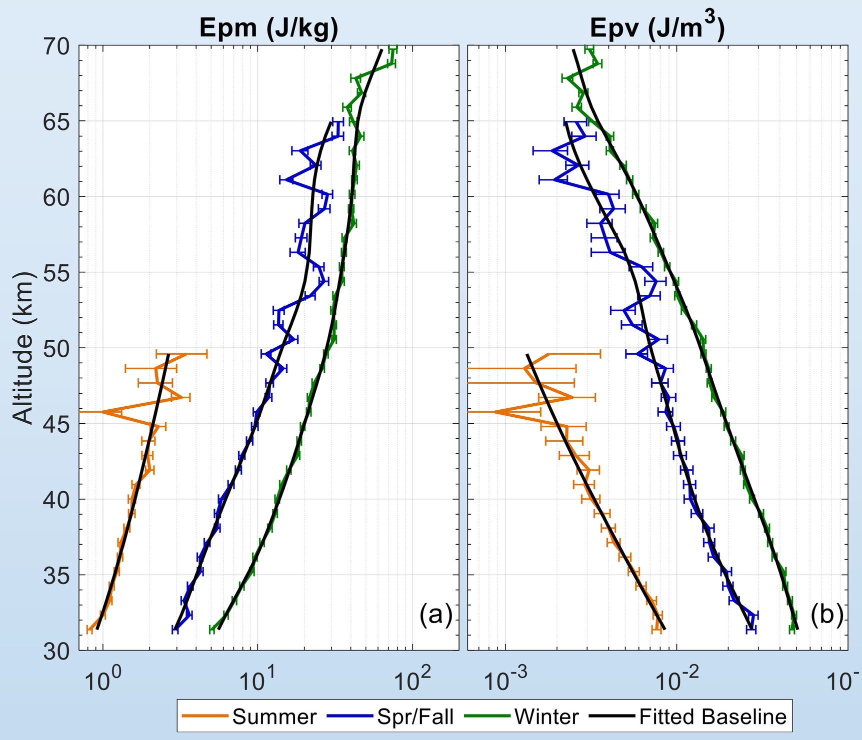

Seasonal Baselines are estimated from 14 yrs of lidar Epm and Epv

Baselines:

- We use 1 km and 1 hr resolution data, with a 2nd order exponential fit + smoothed residual
- Error bars represent statistical and noise-based uncertainties

Observations:

- Expected Epm & Epv seasonal differences appear which Chu et al. (2018) theorize are due to stratospheric wind filtering
- Scale heights (H_{pm}, H_{pv}) vary with altitude and season, with higher H in spring/fall which has not yet been explored
- A few sharp changes in scale height are noted in winter around 39 and 50 km. These are explored further in "…Vertical Lifecycle…"

Assessing Baseline Annual Variations:

- An annual Epm contour plot is created with baselines estimated similarly in each 14-yr monthly average, from 30-50 km (as summers only reach 50 km)
- The AO-SAO function below was fit to all altitudes, and the parameters plotted alongside the contour
- A strong AO is observed, strengthening with altitude
- Minimal SAO is observed in this fitting at any altitude
- AO phase peaks after solstice, and is stable with altitude

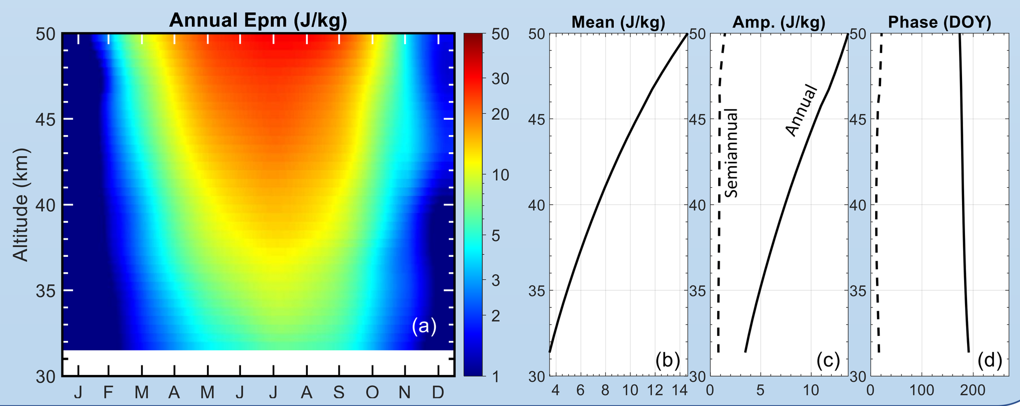

m- and ω-Spectral Baselines

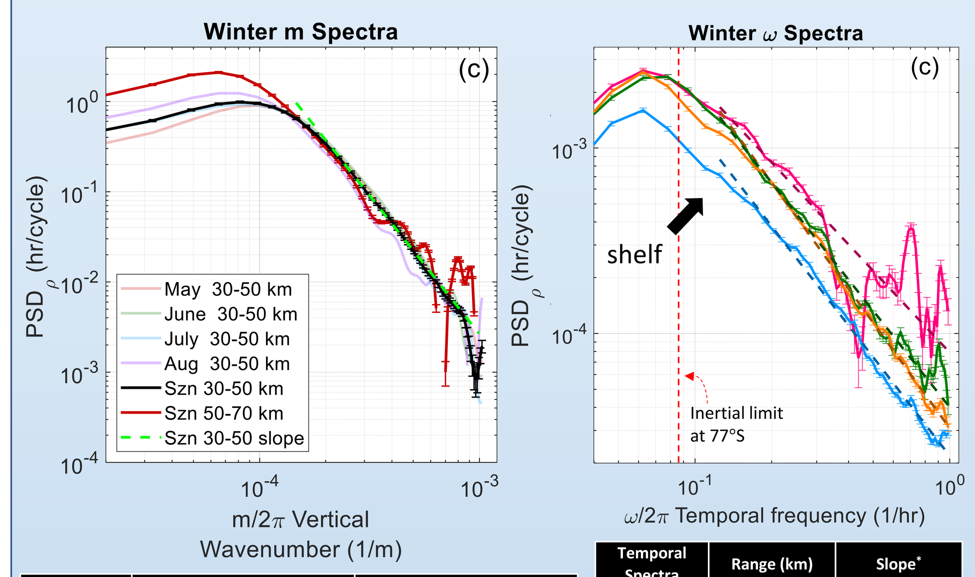

m-spectra	30-50 km		50-70 km	
	Slope*	λ_{z*} (km)	Slope*	λ_{z*} (km)
Summer	-2.62 ± 0.14**	8.7	–	–
Spr/Fall	-2.57 ± 0.03	12.3	-2.93 ± 0.10	12.3
Winter	-3.07 ± 0.02	12.3	-2.73 ± 0.09	15.3

Temporal Spectra	Range (km)	Slope*
Summer	30-40	-1.88 ± 0.12**
	40-50	-2.09 ± 0.80
Spring/Fall	30-40	-1.62 ± 0.01
	40-50	-1.44 ± 0.06
	50-60	-2.19 ± 0.06
	60-70	-1.91 ± 0.19
Winter	30-40	-1.77 ± 0.04
	40-50	-1.89 ± 0.03
	50-60	-1.73 ± 0.05
	60-70	-1.47 ± 0.05

Spring/Fall and Summer Spectral Baselines

- Spr/Fall baselines match many of the winter observations
- Higher uncertainty makes it more difficult to assess trends

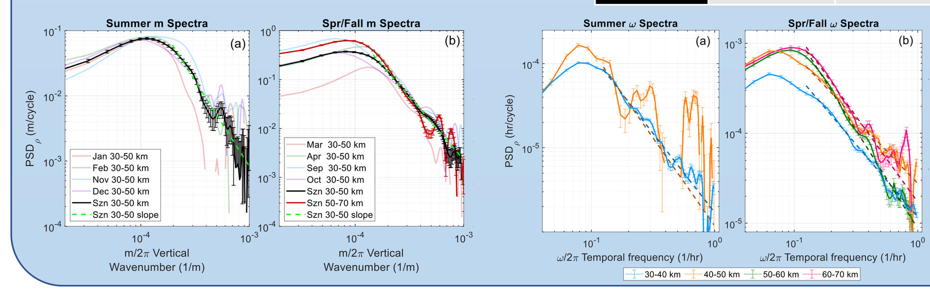

Interpreting the Winter GW Spectra

Processing details:

- m-spectra are estimated at a resolution of 0.5 km and 1 hr, with identical filtering as described in the methodology section of this poster
- ω-spectra are taken at 1 km and 0.5 hr, though temporal filtering uses a 24 hr cutoff to demonstrate that nom-GW energy exists beyond the inertial limit

Observations:

- m-spectra slopes are ~ -3 and ω slopes are $\sim -1.6 - -2$
- PSD(m) increases with altitude only in the low-m region, where PSD(ω) increases nearly-uniformly between adjacent altitude regions
- A minor "shelf" is observed (see ➡) at all altitudes in PSD(ω) around 1/8 hr

Interpretations:

- Theories of saturated (sat) cascade (SCT) and diffusive filtering (DF) could explain many of these features
  - SCT & DF both predict $PSD_{sat}(m) \propto \alpha N_B^2/m^3$. This matches our m-slopes, but our decr. N_B^2 with alt. gives a $PSD_{sat}(m)$ which does not match our $PSD(m)$
  - SCT & DF suggest $PSD_{sat}(\omega) \propto \epsilon/\omega^2$, which matches our slopes. Dissipation rate ϵ is not measured here, yet studies show higher mesospheric ϵ[6], which could explain the uniformly increasing $PSD(\omega)$ with altitude.
  - Plots on the right compare PSD_{sat} est. with reasonable values for α and ϵ. The "disagreement" in $PSD(m)$ may imply unsaturated m-spectra from 30-50 km, and slope is retained from a lower alt (as suggested by others[3]).
- The shelf in ω-spectra has been observed by previous Antarctic observations[4,5,6] in above/below altitude bands
  - May be the GW ω_* obscured by non-GW energy here

PSD_{sat} in Winter GW

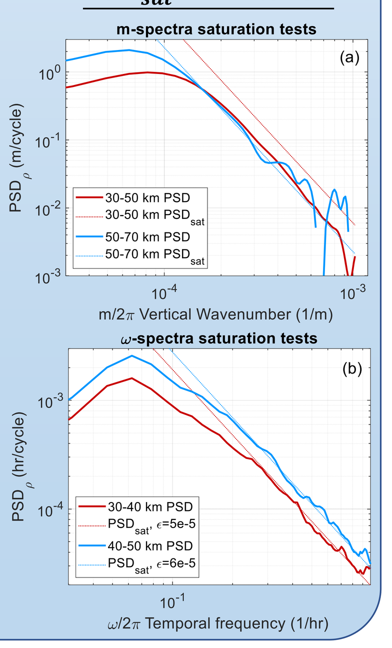

McMurdo GW Vertical Lifecycle

Scale-dependent Dissipation in Middle Atmosphere Winter GW Ep

Observations:

- At 39 and 50 km, GW Epm profiles display a "bending point" (BP), a sharp increase in H_{pm} indicating that GW are dissipating more quickly
- When broken down by scale, it is apparent that small-scale waves ($\lambda_z =$ 2-8 km) show this BP at 39 km and large-scale waves ($\lambda_z = 8-30$ km) show this BP at 50 km

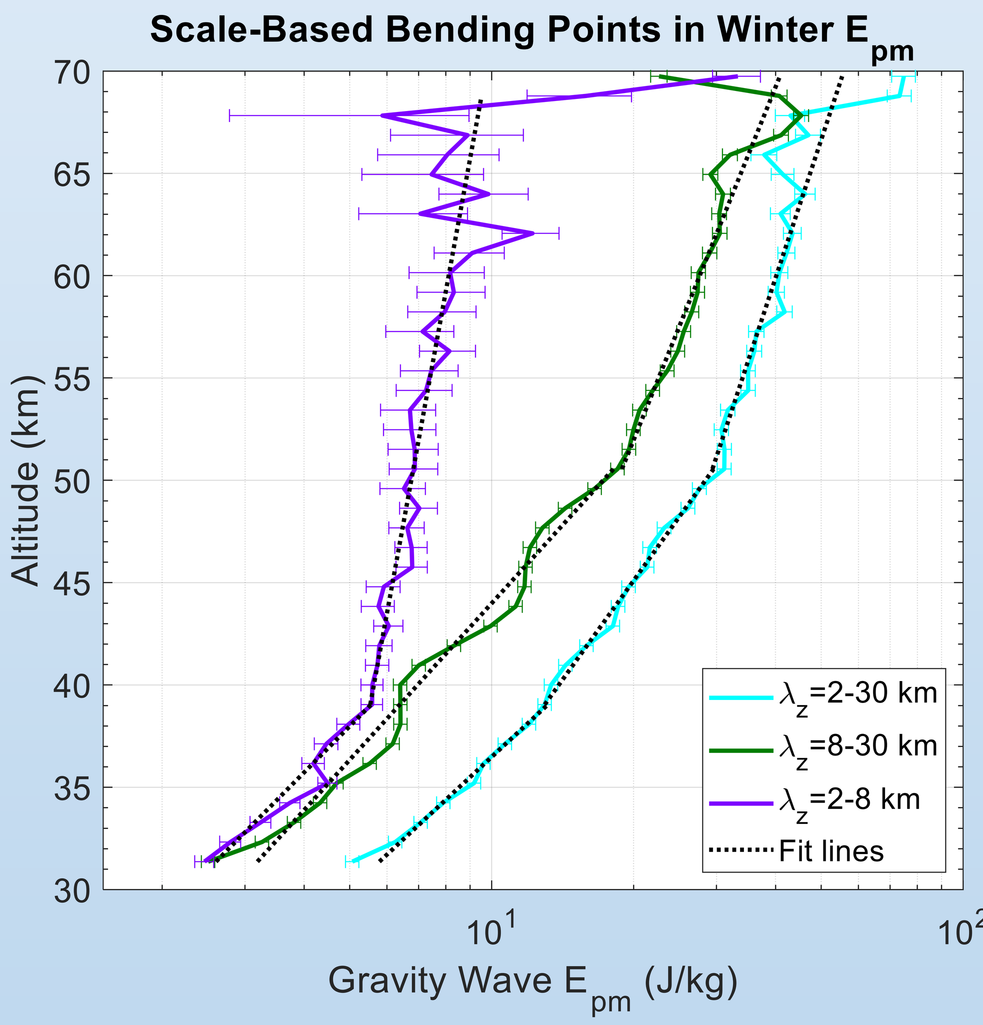

Wavelength Range	Altitude of Fit	H_{pm} (km)
λ_z = 2-30 km	30-39 km	9.3 ± 0.9
	39-50 km	14.0 ± 2.3
	50-68 km	30.3 ± 11.1
λ_z = 2-8 km	30-39 km	10.1 ± 2.0
	39-65 km	54.7 ± 8.9
λ_z = 8-30 km	30-50 km	11.0 ± 0.86

Potential explanations for Bending Points:

While concrete conclusion on the mechanism causing this feature requires more detailed study, we propose a few ideas.

Convective Instability (Hodges, 1967):

- One of the older and more simple explanations of GW breaking, though its simplicity makes it easy to apply
- As upward propagating GW grow alongside decreasing background density, they can grow so strong that they create local convective instabilities, leading to GW breaking
- Convective instability can be expressed by $|u'_H/c_H - u_H| \sim 1$ ($c_H :=$ horizontal phase speed)
  - This c_H gives a scale-dependence; small-scale waves (with smaller c_H) would be unstable at lower u'_H and begin dissipating at lower altitudes than larger-waves
- However, this cannot explain why the BP are at distinct altitudes; the "condition-meeting" should be more gradual

Diffusive Filtering (Gardner, 1994):

- Non-linear interactions between atmospheric diffusion (molecular *and* eddy) act to against the bulk wave motion to degrade and ultimately dissipate the wave
- Strongest when vertical diffusive transport is $\sim \lambda_z$, such that only waves with $m \leq (\omega/D)^{1/2}$ can grow unhindered, meaning that small-scale waves would break at lower alts.
- The scale heights observed above and below the BP agree reasonably with those predicted by Gardner (1994).

Implications of Bending Points:

Without confirmation on the mechanism responsible, we can only speculate on the implications of the localized dissipation.

- Things we know for certain:
  - The waves show regions of increased dissipation, meaning they are generating more heat, turbulence, and wave drag on the atmosphere in this region
  - The altitude of this atmospheric energy deposition is scale dependent. This suggests a dependence of the deposition alt and strength on atmo. filtering and source dependence (smaller-waves deposit energy lower, etc.)
- Possible implications
  - 2 cases of secondary wave generation above McMurdo have been discovered at 43 and 52 km. It is known that strongly localized wave breaking can generate these waves, though this cannot be confidently linked to the BP

Gravity Waves from 80-110 km and Vertical Coupling

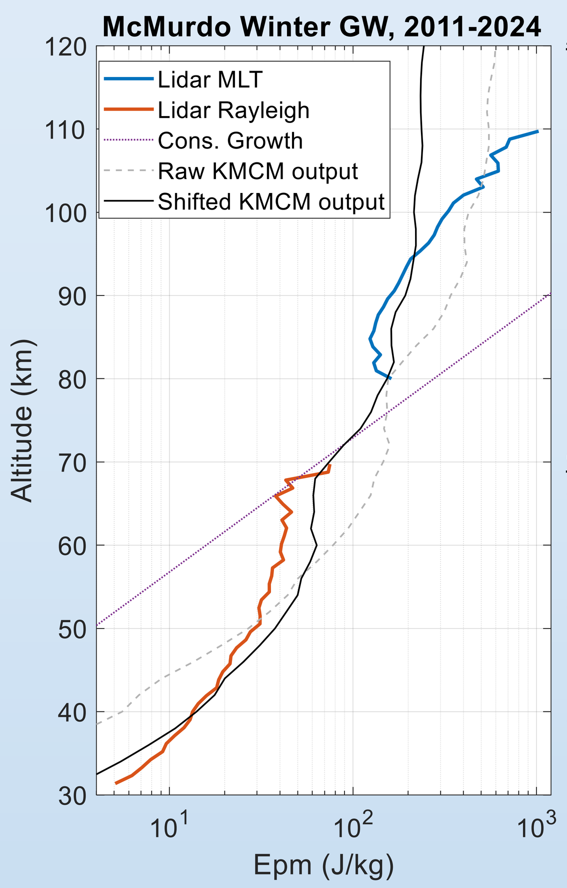

Assessing the MLT Epm

- Due to inherent limitations in the photon return mechanisms, a data gap exists from 70-80 km
- The MLT Epm shows a very large H_{pm} from 80-85 km, from 80-110 km H_{pm} then decreases

Note that these GW often propagate very obliquely, meaning the same GW is unlikely to be observed continuously from 30-110 km. Theories of GW "growth" are intended in a statistical sense.

Comparison with Middle Atmo.

- Alongside MLT Epm, the 65-70 km increasing Epm appear to suggest growth from 70-80 km
- Non-dissipating GW (H=7 km) could grow to complete this gap as shown by the purple line
- GW resolving KMCM model[8] data, sampled-as-McM lidar, show such growth, albeit at a higher altitude (see the shifted curve).

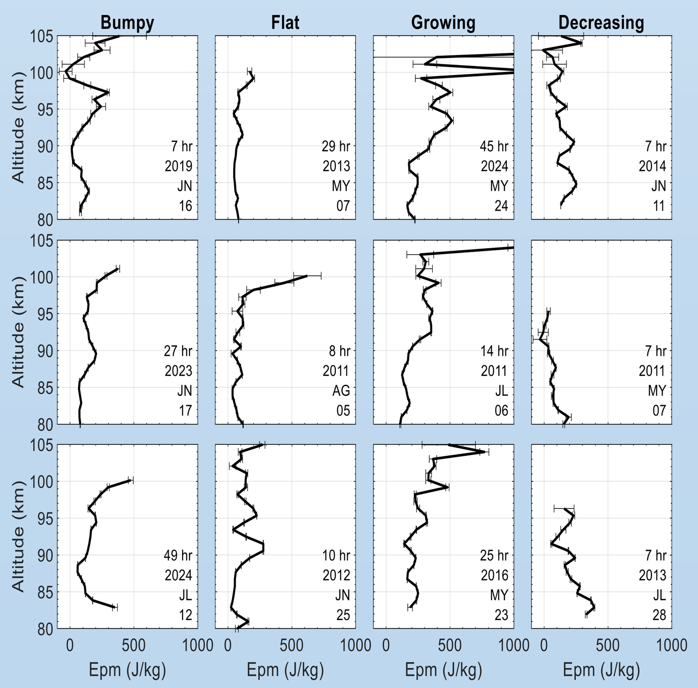

Variability in MLT GW

The MLT Epm averages are complemented by a demonstration of the variability of GW Epm, similarly variable to the strato/mesosphere, but concealed underneath the averaging.

While the intention of baselines is to remove this variability, the baselines are in fact complemented by such examples

Conclusions

- The interleaved method enables significantly more trustworthy E_p and spectral plots, enabling the study of precise features without worry of bias
- Baseline Spring/Fall E_{pv} plots suggest a region of increased wave growth (or decreased dissipation) from 45-55 km, which may be due to reduced filtering
- Vertical wavenumber spectra have similar amplitudes at high wavenumbers for 30-50 km and 50-70 km regions, demonstrating that altitudinal wave growth occurs primarily in the low-m scales
- We can now speculate on the growth of wave between one region to the next, though confirmation requires much more study, and likely will benefit from a model comparison.

Next Steps

Baselines

- Monthly E_{pm} baselines reveal possible turning points in non-winter months, but confirmation requires more careful analysis and possibly additional data
- Assess further links between behavior observed in the spectra to that observed in the energy profiles

Wave Dissipation and Breaking

- Search for evidence of wave breaking in the MLT observations, either fishbone structure or upwards phase progression
- Try and assess observed GW dissipation using GW resolving models
  - See if these models reflect similar dissipative regions and if so, assess the exact cause for this (i.e., confirm if it is breaking)

References

Becker, E., Vadas, S. L., & Chu, X. (n.d.). Multi-step vertical coupling via gravity waves from the lower to the upper atmosphere.
Chen, C., Chu, X., Zhao, J., Roberts, B. R., Yu, Z., Fong, W., et al. (2016). Lidar observations of persistent gravity waves with periods of 3–10 h in the Antarctic middle and upper atmosphere at McMurdo (77.83°S, 166.67°E). *Journal of Geophysical Research: Space Physics*, *121*(2), 1483–1502. https://doi.org/10.1002/2015JA022127
Jandreau, J., & Chu, X. (2022). Comparison of Three Methodologies for Removal of Random-Noise-Induced Biases From Second-Order Statistical Parameters of Lidar and Radar Measurements. *Earth and Space Science*, *9*, e2021EA002073. https://doi.org/10.1029/2021EA002073
Jandreau, J., & Chu, X. (2024). Bias-Eliminating Techniques in the Computation of Power Spectra for Characterizing Gravity Waves: Interleaved Methods and Error Analyses. *Earth and Space Science*, *11*(10), e2023EA003499. https://doi.org/10.1029/2023EA003499
Senft, D. C., & Gardner, C. S. (1991). Seasonal variability of gravity wave activity and spectra in the mesopause region at Urbana. *Journal of Geophysical Research*, *96*(D9), 17229. https://doi.org/10.1029/91JD01662
Vadas, S. L., Zhao, J., Chu, X., & Becker, E. (2018). The Excitation of Secondary Gravity Waves From Local Body Forces: Theory and Observation. *Journal of Geophysical Research: Atmospheres*, *123*(17), 9296–9325. https://doi.org/10.1029/2017JD027970

McMurdo lidar projects are supported by NSF Grants OPP-2110428, Jackson is partially supported by NASA 80NSSC22K1854